Inorg. Chem. **2002**, *41*, 2193–2201

Theoretical Investigation of the Spin Exchange Interactions and Magnetic Properties of the Homometallic Ludwigite $Fe_3O_2BO_3$

M.-H. Whangbo* and H.-J. Koo

Department of Chemistry, North Carolina State University, Raleigh, North Carolina 27695-8204

J. Dumas

Laboratoire d'Etudes des Propiétés Electroniques des Solides, CNRS, BP 166, 38042, Grenoble Cedex 9, France

M. A. Continentino

Instituto de Fisica, Universidade Federal Fuluminense, Campus da Praia Vermelha, Niteroi, 24210-340, Brazil

Received September 6, 2001

The homometallic ludwigite $Fe_3O_2BO_3$ has a complex structure made up of corner- and edge-sharing FeO_6 octahedra and exhibits a number of apparently puzzling magnetic properties. The reasons for these properties were probed by examining the trends in the spin exchange interactions of $Fe_3O_2BO_3$. To analyze the relative strengths of spin exchange interactions in such a complex magnetic solid, we first generalized the method of spin dimer analysis and then employed the resulting formulation to investigate how the magnetic properties of $Fe_3O_2BO_3$ are related to its reported crystal structures. The spin–orbital interaction energies calculated for various spin dimers of $Fe_3O_2BO_3$ provide estimates for the relative strengths of the associated spin exchange interactions, which in turn account for the observed magnetic properties of $Fe_3O_2BO_3$.

1. Introduction

In the ludwigites of general formula $M_2M'O_2BO_3$, the transition metal atoms M and M′ are present as divalent and trivalent cations, respectively.[1−6] Thus, the homometallic ludwigite $Fe_3O_2BO_3$ is a mixed valence iron compound with one Fe^{3+} and two Fe^{2+} ions per formula unit. $Fe_3O_2BO_3$ exhibits a number of interesting physical properties,[6−11] and the charge distribution of $Fe_3O_2BO_3$ was examined in terms of electronic structure calculations in one report.[12] $Fe_3O_2BO_3$ is a semiconductor with activation energy $E_a = 5.2$ and 112 meV above and below ∼220 K.[6] Recently, Mir et al. showed that $Fe_3O_2BO_3$ undergoes a structural transition at 283 K and characterized this transition by determining the crystal structure at temperatures above and below 283 K (i.e., at 294 and 144 K, respectively).[7] According to the Mössbauer spectroscopy study, the Fe^{2+} and Fe^{3+} ions of $Fe_3O_2BO_3$ are

* To whom correspondence should be addressed. E-mail: mike_whangbo@ncsu.edu.

(1) Schaefer, J.; Bluhm, K. *Z. Anorg. Allg. Chem.* **1995**, *621*, 571.
(2) Continentino, M. A.; Fernandes, J. C.; Guimarães, R. B.; Borges, H. A.; Sulpice, A.; Tholance, J.-L.; Siqueira, J.; da Cunha, J. B. M.; dos Santos, C. A. *Eur. Phys. J. B* **1999**, *9*, 613.
(3) Perkins, D. A.; Attfield, J. P. *J. Chem. Soc., Chem. Commun*. **1991**, 229.
(4) Fernandes, J. C.; Guimarães, R. B.; Continentino, M. A.; Borges, H. A.; Sulpice, A.; Tholance, J.-L.; Siqueira, J.; Zawislak, L. I.; da Cunha, J. B. M.; dos Santos, C. A. *Phys. Rev. B* **1998**, *58*, 287.
(5) Swinnea, J. S.; Steinfink, H. *Am. Mineral*. **1983**, *68*, 827.
(6) Guimarães, R. B.; Mir, M.; Fernandes, J. C.; Continentino, M. A.; Borges, H. A.; Cernicchiaro, G.; Fontes, M. A.; Candela, D. R. S.; Baggio-Saitovitch, E. M. *Phys. Rev. B* **1999**, *60*, 6617.
(7) Mir, M.; Guimarães, R. B.; Fernandes, J. C.; Continentino, M. A.; Doriguetto, A. C.; Mascarenhas, Y. P.; Ellena, J.; Castellano, E. E.; Freitas, R. S.; Ghivelder, L. *Phys. Rev. Lett*. **2001**, *87*, 147201.
(8) Fernandes, J. C.; Guimarães, R. B.; Mir, M.; Continentino, M. A.; Borges, H. A.; Cernicchiaro, G.; Fontes, M. A.; Baggio-Saitovitch, E. M. *Physica B* **2000**, *281/282*, 694.
(9) Fernandes, J. C.; Guimarães, R. B.; Continentino, M. A. *Phys. Rev. B* **2000**, *61*, R850.
(10) Dumas, J.; Tholance, J.-L.; Continentino, M. A.; Fernandes, J. C.; Guimarães, R. B. *J. Magn. Magn. Mater*. **2001**, *226/230*, 468.
(11) Larrea, J. A.; Sánchez, D. R.; Baggio-Saitovitch, E. M.; Fernandes, J. C.; Guimarães, R. B.; Continentino, M. A.; Litterst, F. J. To be published.
(12) Matos, M.; Anda, E. V.; Fernandes, J. C.; Guimarães, R. B. *THEOCHEM* **2001**, *539*, 181.

10.1021/ic010956q CCC: $22.00
Published on Web 03/14/2002

in the high-spin states ($S = 2$ and $^5/_2$, respectively),[6,11] so $Fe_3O_2BO_3$ is a magnetic semiconductor. Upon lowering temperature, $Fe_3O_2BO_3$ undergoes an antiferromagnetic transition at $T_N = 112$ K and exhibits a weak ferromagnetism below $T_c = 70$ K.[6] Below 40 K, the spontaneous magnetization disappears, and $Fe_3O_2BO_3$ becomes antiferromagnetic again.[6] Between 112 and 70 K, antiferromagnetism and paramagnetism coexist.[6] Guimarães et al.[6] suggested that $Fe_3O_2BO_3$ has two spin sublattices, that is, the sublattice of the Fe(4)−Fe(2)−Fe(4) edge-sharing triads and that of the Fe(3)−Fe(1)−Fe(3) corner-sharing triads (in the atom numbering scheme of Swinnea and Steinfink[5] and Mir et al.,[7] see section 2), and these two sublattices are decoupled to a first approximation.

Concerning the physical properties of $Fe_3O_2BO_3$, a number of important questions remain unexplored. (a) What electronic factor causes the occurrence of the two weakly interacting spin sublattices? (b) The antiferromagnetic transition at T_N takes place in the sublattice of the Fe(4)−Fe(2)−Fe(4) triads.[6] Then, how do adjacent Fe(4)−Fe(2)−Fe(4) triads interact to have a three-dimensional (3D) antiferromagnetic ordering? (c) This 3D antiferromagnetic ordering is not seen by the magnetic susceptibility measurements.[6] Why? (d) It has been suggested[6] that the weak ferromagnetism at T_c arises from the Fe(3)−Fe(1)−Fe(3) sublattice and is induced by a canting of antiferromagnetically ordered spins. Then, how does this ferromagnetism disappear below 40 K? (e) The EPR study shows[10] that $Fe_3O_2BO_3$ has a single broad line associated with the Fe^{2+} ions and its peak-to-peak line width decreases gradually with increasing the temperature above 70 K. What is the origin of this unconventional temperature dependence? To answer these questions, one must investigate how the observed physical properties of $Fe_3O_2BO_3$ are related to its crystal structures determined above and below the structural phase transition temperature 283 K (i.e., at room temperature and 144 K[7]). To understand how the observed physical properties of $Fe_3O_2BO_3$ are related to its crystal structures, it is essential to carry out appropriate electronic structure calculations for the observed crystal structures of $Fe_3O_2BO_3$.

Theoretically, physical properties of a magnetic solid are described in terms of a spin-Hamiltonian, which is expressed as a sum of pairwise spin exchange interactions between adjacent spin sites.[13] There are two ways of determining the strengths of spin exchange interactions (i.e., spin exchange parameters J) on the basis of first-principles electronic structure calculations. One is based on electronic structure calculations for the high- and low-spin states of spin dimers (i.e., structural units consisting of two spin sites),[14−16] and the other is based on electronic band structure calculations for various ordered spin arrangements of a magnetic solid.[17] For a structurally complex magnetic solid such as $Fe_3O_2BO_3$ (see section 2), these quantitative methods are difficult to apply. In understanding structure−property relationships of magnetic solids, however, it is often sufficient to estimate the relative strengths of spin exchange interactions. For a number of magnetic solids, it has been shown[18−26] that trends in spin exchange interactions are reasonably well reproduced in terms of the spin−orbital interaction energies calculated for their spin dimers using the extended Hückel method.[27] In the present work, this spin dimer analysis will be employed to investigate the trends in the spin exchange interactions of $Fe_3O_2BO_3$. For this purpose, it is necessary to generalize the method of spin dimer analysis so that one can calculate spin−orbital interaction energies of spin dimers in which the two octahedral spin sites possess different numbers of unpaired spins.

Our work is organized as follows: The essential features of the reported crystal structures of $Fe_3O_2BO_3$ at room temperature and 144 K are described in section 2. The method of spin dimer analysis is generalized in section 3. The resulting formulas are used in section 4 to calculate the spin−orbital interactions energies for various nearest-neighbor spin exchange interactions in $Fe_3O_2BO_3$. The observed magnetic properties of $Fe_3O_2BO_3$ are then discussed on the basis of these calculations in section 5. The essential findings of our work are summarized in section 6.

2. Crystal Structures, Iron Oxidation States and Charge Ordering

For our description of the magnetic properties of $Fe_3O_2BO_3$, it is essential to discuss its crystal structures[5,7] above and below the structural phase transition temperature, 283 K. $Fe_3O_2BO_3$ can be considered as constructed from FeO_4 octahedral chains made up of trans edge-sharing FeO_6 octahedra (Figure 1). The FeO_4 chains of $Fe_3O_2BO_3$ run along the c-direction and share their edges to form zigzag walls perpendicular to the ab-plane (Figure 2a), which leads to four crystallographically different iron sites, Fe(i) ($i = 1-4$). Two structural features of $Fe_3O_2BO_3$ critical for our discussion are that each Fe(2)O_4 chain is edge-shared with two adjacent Fe(4)O_4 chains to form chains of the edge-sharing Fe(4)−Fe(2)−Fe(4) triads (Figure 2b) and that each Fe(1)O_4 chain is corner-shared with two adjacent Fe(3)O_4 chains to form chains of corner-sharing Fe(3)−Fe(1)−Fe(3) triads (Figure 2c). It is also convenient to regard $Fe_3O_2BO_3$ as constructed from the "Fe/O" layers, parallel to the ab-plane,

(13) Kahn, O. *Molecular Magnetism*; VCH Publishers: Weinheim, Germany, 1993.
(14) Illas, F.; Moreira, I. de P. R.; de Graaf, C.; Barone, V. *Theor. Chem. Acc.* **2000**, *104*, 265 and references therein.
(15) Noodleman, L. *J. Chem. Phys.* **1981**, *74*, 5737.
(16) Dai, D.; Whangbo, M.-H. *J. Chem. Phys.* **2001**, *114*, 2887.
(17) Derenzo, S. E.; Klitenberg, M. K.; Weber, M. J. *J. Chem. Phys.* **2000**, *112*, 2074 and references therein.
(18) Lee, K.-S.; Koo, H.-J.; Whangbo, M.-H. *Inorg. Chem.* **1999**, *38*, 2199.
(19) Koo, H.-J.; Whangbo, M.-H. *Solid State Commun.* **1999**, *111*, 353.
(20) Whangbo, M.-H.; Koo, H.-J.; Lee, K.-S. *Solid State Commun.* **2000**, *114*, 27.
(21) Koo, H.-J.; Whangbo, M.-H. *J. Solid State Chem.* **2000**, *151*, 96.
(22) Koo, H.-J.; Whangbo, M.-H. *J. Solid State Chem.* **2000**, *153*, 263.
(23) Koo, H.-J.; Whangbo, M.-H. *Inorg. Chem.* **2000**, *39*, 3599.
(24) Koo, H.-J.; Whangbo, M.-H.; Coste, S.; Jobic, S. *J. Solid State Chem.* **2001**, *156*, 464.
(25) Koo, H.-J.; Whangbo, M.-H. *Inorg. Chem.* **2001**, *40*, 2169.
(26) Dai, D.; Koo, H.-J.; Whangbo, M.-H. In *Solid State Chemistry of Inorganic Materials*, MRS Symposium Proceedings; Geselbracht, M. J., Greedan, J. E., Johnson, D. C., Subramanian, M. A., Eds.; Materials Research Society: Warrendale, PA; Vol. 658; GG5.3.1−5.3.11.
(27) Hoffmann, R. *J. Chem. Phys.* **1963**, *39*, 1397.

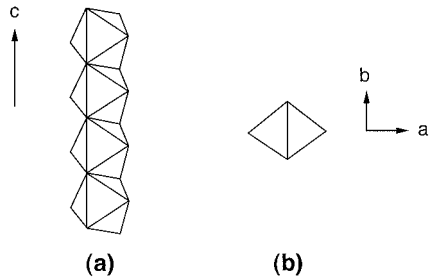

Figure 1. (a) Perspective view of an edge-sharing FeO_4 octahedral chain in polyhedral representation. (b) Projection view of an edge-sharing FeO_4 octahedral chain along the chain direction in polyhedral representation.

made up of edge- and corner-sharing FeO_6 octahedra. The projection view of this Fe/O layer along the *c*-direction is also given by Figure 2a. The structure of $Fe_3O_2BO_3$ is obtained when adjacent Fe/O layers are condensed by sharing the edges of their FeO_6 octahedra.

In the room-temperature crystal structure of $Fe_3O_2BO_3$, the Fe(4)−Fe(2)−Fe(4) triads form three leg ladders (3LL) of iron atoms running along the *c*-direction (Figure 3a), where the Fe(4)−Fe(2) distance is 2.786 Å. In the crystal structure of $Fe_3O_2BO_3$ below 283 K, the Fe atoms are no longer symmetrically related as depicted in Figure 3b. The Fe(2) atom in each rung is shifted from the central position such that Fe(4a)−Fe(2) = 2.616 Å and Fe(4b)−Fe(2) = 2.942 Å at 144 K.

In estimating the spin exchange interactions of $Fe_3O_2BO_3$, one needs to calculate the electronic structures for their spin dimers and spin monomers (i.e., structural units containing one spin site) (section 3). The spin monomers of $Fe_3O_2BO_3$ are given by the FeO_6 octahedral clusters. A spin dimer consists of two spin monomers and hence is given by an Fe_2O_{12} cluster if the two spin monomers do not share any oxygen atoms. A spin dimer is given by Fe_2O_{11} and Fe_2O_{10} clusters when the spin monomers share an octahedral corner and edge, respectively.

The iron oxidation states of $Fe_3O_2BO_3$ can be estimated by calculating the bond valence sum for each Fe(*i*) ($i = 1-4$) atom on the basis of the six Fe−O bonds of each Fe(*i*)O_6 octahedron. For oxides of a transition metal atom M, the bond valence v_i of its M−O bond with length r_i is defined as $v_i = \exp[(r_i - r_0)/0.370]$, where r_0 is the reference bond length.[28] The bond valence v_i has the meaning of the electron density the atom M lost to form the M−O bond, so that the sum of the bond valences for all the M−O bonds surrounding the atom M is the oxidation state of M. The reference Fe−O bond length r_0 is 1.759 Å for an Fe^{3+} ion and 1.734 Å for an Fe^{2+} ion.[28] Table 1 summarizes the two sets of bond valence sums calculated using these two r_0 values. It is clear that the oxidation states of Fe(1) and Fe(3) should be regarded as +2. In the room temperature structure, the oxidation state of Fe(2) is slightly higher than +2, but lower than +2.5. The oxidation state of Fe(4) is higher than that of Fe(2) and is lower than +3. Thus, at room temperature, it is reasonable to assign the oxidation states of Fe(2) and Fe(4) as +2 and +3, respectively. As the temperature is

(28) Brese, N. E.; O'Keefe, M. *Acta Crystallogr. B* **1991**, *47*, 192.

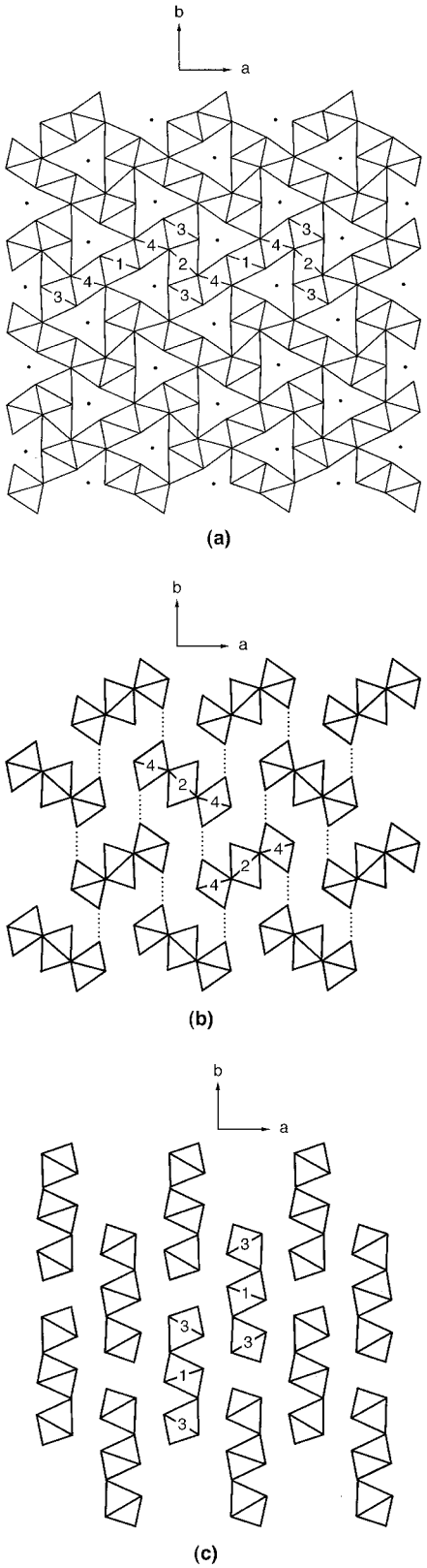

Figure 2. Projection views in polyhedral representation, along the direction of the edge-sharing FeO_4 octahedral chain, of (a) the structure of $Fe_3O_2BO_3$, (b) the chains of the Fe(4)−Fe(2)−Fe(4) edge-sharing triads in $Fe_3O_2BO_3$, and (c) the chains of the Fe(3)−Fe(1)−Fe(3) corner-sharing triads in $Fe_3O_2BO_3$. In (a), the boron atoms are represented by heavy dots, and the octahedra with numbers *i* (=1−4) indicate that they have the Fe(*i*) atoms. In (b), the dotted lines indicate the O···O contacts involved in the Fe(4)−O···O−Fe(4) super-superexchange paths between adjacent Fe(4)−Fe(2)−Fe(4) triads.

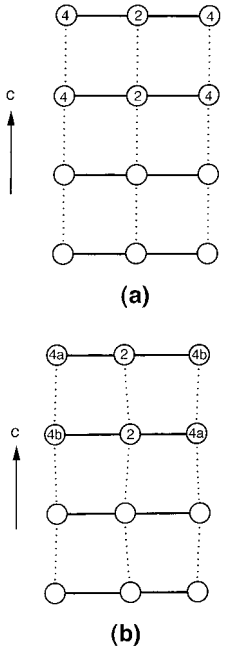

Figure 3. Schematic representations of a three leg ladder of iron atoms made up of the Fe(4)−Fe(2)−Fe(4) triads above (a) and below (b) the structural phase transition temperature.

lowered below 283 K, the oxidation states of Fe(2) and Fe(4b) increase slightly, while that of Fe(4a) decreases slightly, such that the Fe(2) and Fe(4a) atoms have a similar oxidation state. Provided that the oxidation state of Fe(4b) is assigned as +3, those of Fe(2) and Fe(4a) become +2.5. Thus, if each Fe(4a)−Fe(2)−Fe(4b) rung is regarded as a unit containing three Fe^{3+} cations and one electron, then the 144 K crystal structure indicates that the extra electron is accommodated by the Fe(2)−Fe(4a) pair of each rung.

It is of interest to consider why the electrical conductivity of $Fe_3O_2BO_3$ shows a sharp increase in activation energy as the temperature is lowered below ~220 K.[6] Although the Fe(2) site is the preferred site for the extra electron in each rung of three Fe^{3+} cations, the Fe(4) sites may also accommodate this electron above ~220 K, probably because of the breathing mode vibrations involving the Fe(4) and Fe(2) sites. If such vibrations are frozen below ~220 K, only the Fe(2)−Fe(4a) pair of each rung may accommodate the extra electron. Consequently, the activation energy for electron hopping in the Fe(4)−Fe(2)−Fe(4) sublattice will become considerably greater below 220 K.

3. Spin Dimer Analysis

The spin exchange parameter J for a given spin dimer consists of ferromagnetic and antiferromagnetic components, $J = J_F + J_{AF}$. Consider the case when each spin site of a magnetic solid contains one unpaired electron under the assumption that the two spin sites of a spin dimer are equivalent and the two spin sites of a spin dimer are represented by nonorthogonal magnetic orbitals (i.e., singly occupied molecular orbitals of the spin monomers) ϕ_1 and ϕ_2. Provided that S_{12} is the overlap integral between ϕ_1 and ϕ_2, and Δe the spin−orbital interaction energy (i.e., the energy separation between the highest two singly occupied

Table 1. Bond Valence Sums Calculated for the Fe(i) Atoms in the 294 and 144 K Structures of $Fe_3O_2BO_3$

Fe(i)	294 K[a]	144 K[a]
Fe(1)	2.17/2.02	2.19/2.05
Fe(2)	2.44/2.28	2.47/2.31
Fe(3)	2.19/2.04	2.20/2.06
Fe(4)	2.67/2.50	2.51/2.35[b]
		2.84/2.65[c]

[a] The numbers in the first column were calculated using the r_0 value for Fe^{3+}, and those in the second column using the r_0 value for Fe^{2+}. [b] For the Fe(4a) atom. [c] For the Fe(4b) atom.

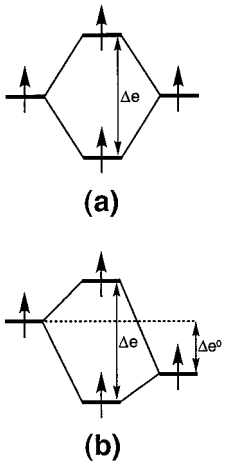

Figure 4. (a) Spin−orbital interaction energy $\Delta\epsilon = \Delta e$ of a spin dimer with two equivalent spin sites. (b) Spin−orbital interaction energy $\Delta\epsilon = \Delta e - \Delta e^0$ of a spin dimer with two nonequivalent spin sites.

energy levels of a spin dimer, Figure 4a), then the antiferromagnetic term J_{AF} (<0) is related to S_{12} and Δe as $J_{AF} \propto -S_{12}\Delta e \propto -(\Delta e)^2$, where the second relationship results from $\Delta e \propto S_{12}$.[13] In general, the ferromagnetic term J_F is small (see later) so that the spin exchange interaction becomes ferromagnetic (i.e., $J > 0$) only when the antiferromagnetic J_{AF} is negligibly small in magnitude. In addition, spin exchange interactions of magnetic solids are mostly antiferromagnetic (i.e., $J < 0$). Therefore, in most cases, one can discuss spin exchange interactions of magnetic solids by focusing on the antiferromagnetic terms J_{AF}.[18−26]

In the case when the two spin sites of a spin dimer are nonequivalent (Figure 4b), the extent of the spin exchange interaction can be estimated by calculating the net spin−orbital interaction energy, $\Delta e - \Delta e^0$, where Δe^0 is the energy difference between the two nonequivalent magnetic orbitals. The Δe^0 value can be estimated from the energies of the magnetic orbitals calculated for the spin monomers representing the two spin sites.[20] Obviously, $\Delta e^0 = 0$, when the two spin sites are equivalent. For the simplicity of our notation, we will use the symbol $\Delta\epsilon$ to represent Δe for the case of two equivalent spin sites, and $\Delta e - \Delta e^0$ for the case of two nonequivalent spin sites.

When two adjacent spin sites have M and N unpaired spins, respectively, the overall spin exchange parameter J is then described by[29]

$$J = \frac{1}{MN}\sum_{\mu=1}^{M}\sum_{\nu=1}^{N} J_{\mu\nu} \qquad (1)$$

so that the trends in spin exchange parameters can be discussed in terms of the average spin−orbital interaction energies defined by[24,26]

$$\langle \Delta\epsilon \rangle = \frac{1}{MN} \sum_{\mu=1}^{M} \sum_{\nu=1}^{N} \Delta\epsilon_{\mu\nu} \tag{2}$$

From the viewpoint of nonorthogonal magnetic orbitals, the antiferromagnetic contribution of each term $\Delta\epsilon_{\mu\nu}$ is zero when the magnetic orbitals ϕ_μ and ϕ_ν are different in symmetry so that $S_{\mu\nu} = 0$ and is negligible when ϕ_μ and ϕ_ν are different in shape so that $S_{\mu\nu}$ is negligibly small. Therefore, only the "diagonal" terms $\Delta\epsilon_{\mu\mu}$ are important in eq 2.[24,26] Let us examine how this finding simplifies eq 2 for cases when each spin site has a transition metal ion in an octahedral environment.

Let us generalize the method of spin dimer analysis[18−26] to enable the calculation of the spin−orbital interaction energies for those spin dimers in which the octahedral spin sites can have different numbers of unpaired spins. First, consider that the two spin sites of a spin dimer have high-spin d^5 ions (i.e., $M = N = 5$) as in the case of two adjacent high-spin Fe^{3+} ($S = {}^5/_2$) ions in $Fe_3O_2BO_3$. Then, the d-electron configuration of each spin site is $(t_{2g})^3(e_g)^2$, so each spin site has three magnetic orbitals (ϕ_1, ϕ_2, and ϕ_3) from the t_{2g}-block levels and two magnetic orbitals (ϕ_4 and ϕ_5) from the e_g-block levels. In terms of these magnetic orbitals, the $(t_{2g})^3(e_g)^2$ configuration is expressed as $(\phi_1)^1(\phi_2)^1(\phi_3)^1(\phi_4)^1(\phi_5)^1$. Thus, the $\langle \Delta\epsilon \rangle$ value for the spin exchange interaction between two adjacent Fe^{3+} ($S = {}^5/_2$) ions in $Fe_3O_2BO_3$ is written as

$$\langle \Delta\epsilon \rangle \approx \frac{1}{5 \times 5} \sum_{\mu=1}^{5} \Delta\epsilon_{\mu\mu} \tag{3}$$

We now consider the spin exchange interactions between spin sites containing different numbers of unpaired spins ($M \neq N$) as in the case of adjacent Fe^{3+} ($S = {}^5/_2$) and Fe^{2+} ($S = 2$) ions in $Fe_3O_2BO_3$. For this purpose, it is convenient to define the following energy terms

$$\Delta\epsilon(t_{2g}) = \Delta\epsilon_{11} + \Delta\epsilon_{22} + \Delta\epsilon_{33}$$

$$\Delta\epsilon(e_g) = \Delta\epsilon_{44} + \Delta\epsilon_{55} \tag{4}$$

The electron configuration of a high-spin Fe^{2+} ($S = 2$) ion is given by $(t_{2g})^4(e_g)^2$. From the viewpoint of the magnetic orbitals ϕ_μ ($\mu = 1-5$), the three configurations $(\phi_1)^2(\phi_2)^1(\phi_3)^1(\phi_4)^1(\phi_5)^1$, $(\phi_1)^1(\phi_2)^2(\phi_3)^1(\phi_4)^1(\phi_5)^1$, and $(\phi_1)^1(\phi_2)^1(\phi_3)^2(\phi_4)^1(\phi_5)^1$ should contribute equally to $(t_{2g})^4(e_g)^2$ if the three orbitals ϕ_1, ϕ_2, and ϕ_3 are degenerate. The spin exchange between adjacent Fe^{2+} ($S = 2$) and Fe^{3+} ($S = {}^5/_2$) ions results only from interactions between singly filled orbitals. Thus, the $\langle \Delta\epsilon \rangle$ value for the spin exchange interaction between adjacent Fe^{2+} ($S = 2$) and Fe^{3+} ($S = {}^5/_2$) ions is expressed as

$$\langle \Delta\epsilon \rangle \approx \frac{1}{4 \times 5}\left[\frac{2}{3}\Delta\epsilon(t_{2g}) + \Delta\epsilon(e_g)\right] \tag{5}$$

This result can be further generalized to a more complex situation. Assume that one spin site has m_t and m_e unpaired spins in the t_{2g}- and e_g-block levels, respectively ($M = m_t + m_e$), while the other spin site has n_t and n_e unpaired spins in the t_{2g}- and e_g-block levels, respectively ($N = n_t + n_e$). Then, it is straightforward to show that the $\langle \Delta\epsilon \rangle$ value is written as

$$\langle \Delta\epsilon \rangle \approx \frac{1}{MN}\left[\frac{m_t}{3} \times \frac{n_t}{3}\Delta\epsilon(t_{2g}) + \frac{m_e}{2} \times \frac{n_e}{2}\Delta\epsilon(e_g)\right] \tag{6}$$

provided that the three t_{2g}-block levels are degenerate and so are the two e_g-block levels.

4. Calculations of Spin−Orbital Interaction Energies

In the present section, we calculate the spin−orbital interaction energy $\langle \Delta\epsilon \rangle$ values for the various nearest-neighbor spin exchange interactions of $Fe_3O_2BO_3$ using the extended Hückel method.[27,30] It has been shown[18−26] that trends in the spin exchange interactions of various magnetic solids are well reproduced when the spin−orbital interaction energies are calculated using double-ζ Slater type orbitals[31] for both the transition-metal d- and the ligand s/p-orbitals. The atomic orbital parameters of Fe and O employed in our calculations are summarized in Table 2.

In calculating the spin−orbital interaction energies $\langle \Delta\epsilon \rangle$ for the room-temperature structure of $Fe_3O_2BO_3$, we employed the oxidation state +2 for the Fe(1), Fe(2), and Fe(3) atoms and the oxidation state +3 for the Fe(4) atom. The room-temperature crystal structure of Swinnea and Steinfink[5] is very similar to that of Mir et al.,[7] so the two structures lead essentially to the same $\langle \Delta\epsilon \rangle$ values. Since we will discuss how these values are affected by the structural transition at 283 K, we report our calculations only for the crystal structures of Mir et al.[7]

The spin exchange interactions calculated for the room-temperature crystal structure are summarized in Table 3. The $\langle \Delta\epsilon \rangle$ values along the FeO_4 octahedral chains (i.e., intrachain spin exchange interactions) are listed at the top of Table 3, and those within each Fe/O layer parallel to the *ab*-plane (i.e., intralayer spin exchange interactions) at the bottom of Table 3. In calculating the $\langle \Delta\epsilon \rangle$ values for the 144 K crystal structure, we employed the oxidation state +2 for Fe(1) and Fe(3) and the oxidation state +3 for Fe(4b). As pointed out in section 2, it is appropriate to consider the oxidation state +2.5 for both Fe(2) and Fe(4a). Thus, we carried out calculations of $\langle \Delta\epsilon \rangle$ in two ways: one with the oxidation states +3 and +2 for Fe(4a) and Fe(2), respectively, and the other with the opposite assignment. As summarized in Table 4, the spin exchange interactions are not much affected by these two different choices. The $\langle \Delta\epsilon \rangle$ values along the

(29) Charlot, M. F.; Kahn, O. *Nouv. J. Chim.* **1980**, *4*, 567.

(30) Our calculations were carried out by employing the *CAESAR* program package (Ren, J.; Liang, W.; Whangbo, M.-H. *Crystal and Electronic Structure Analysis Using CAESAR*; 1998, http://www.PrimeC.com/).

(31) Clementi, E.; Roetti, C. *Atomic Data Nuclear Data Tables* **1974**, *14*, 177.

Table 2. Exponents ζ_i and Valence Shell Ionization Potentials H_{ii} of Slater Type Orbitals χ_i Used for Extended Hückel Tight-Binding Calculation[a]

atom	χ_i	H_{ii} (eV)	ζ_i	c_1[b]	$\zeta_{i'}$	c_2[b]
Fe	4s	−9.10	1.925	1.0		
Fe	4p	−5.30	1.390	1.0		
Fe	3d	−12.6	6.068	0.4038	2.618	0.7198
O	2s	−32.3	2.688	0.7076	1.675	0.3745
O	2p	−14.8	3.694	0.3322	1.659	0.7448

[a] H_{ii}'s are the diagonal matrix elements $\langle\chi_i|H^{\text{eff}}|\chi_i\rangle$, where H^{eff} is the effective Hamiltonian. In our calculations of the off-diagonal matrix elements $H^{\text{eff}} = \langle\chi_i|H^{\text{eff}}|\chi_j\rangle$, the weighted formula was used. See: Ammeter, J.; Bürgi, H.-B.; Thibeault, J.; Hoffmann, R. *J. Am. Chem. Soc*. **1978**, *100*, 3686. [b] Coefficients used in the double-ζ Slater type orbital expansion.

Table 3. Structural Features and Spin−Orbital Interaction Energies $\langle\Delta\epsilon\rangle$ of Various Spin Dimers in the 294 K Structure of $Fe_3O_2BO_3$

spin dimer	Fe···Fe (Å) (O···O)	interaction	oxygen sharing	$\langle\Delta\epsilon\rangle$ (meV)
Interactions along the FeO_4 Octahedral Chains				
Fe(1)−Fe(1)	3.075	intrachain	edge	15.6
Fe(2)−Fe(2)	3.075	intrachain	edge	16.3
Fe(3)−Fe(3)	3.075	intrachain	edge	16.0
Fe(4)−Fe(4)	3.075	intrachain	edge	13.2
Interactions within Each Fe/O Layer				
Within the Fe(4)−Fe(2)-Fe(4) Sublattice				
Fe(2)−Fe(4)	2.786	intratriad	edge	14.0
Fe(4)−Fe(4)	6.155 (2.379)	intertriad	none	4.9
Within the Fe(3)−Fe(1)-Fe(3) Sublattice				
Fe(1)−Fe(3)	3.376	intratriad	corner	6.7
Fe(3)−Fe(3)	4.769 (2.384)	intertriad (//a)	none	1.3
Fe(3)−Fe(3)	5.557 (2.883)	intertriad (//b)	none	0.7
Between the two Sublattices				
Fe(1)−Fe(4)	3.103	intersublattice	edge	2.0
Fe(2)−Fe(3)	3.176	intersublattice	edge	2.9
Fe(3)−Fe(4)	3.189	intersublattice	edge	2.4
Fe(3)−Fe(4)	3.416	intersublattice	corner	5.8

FeO_4 octahedral chains (i.e., intrachain spin exchange interactions) are listed at the top of Table 4, and those within each Fe/O layer parallel to the *ab*-plane (i.e., intralayer spin exchange interactions) at the bottom of Table 4.

Our results do not change when calculations are carried out with spin dimers including BO_3 units. That is, the B−O bonds are not important as spin exchange paths. The same conclusion was reached in our study[32] of another magnetic solid containing BO_3 units, that is, $SrCu_2(BO_3)_2$.[33,34] As shown earlier,[18,23,25] it is important to notice that spin exchange in a transition metal oxide can take place through super-superexchange paths, M−O···O−M, and these paths can provide a stronger spin exchange coupling than do superexchange paths, M−O−M (here, M represents a transition metal atom, and O···O a nonbonded oxygen−oxygen contact).

For magnetic solids containing one unpaired spin per spin site, it is not difficult to provide simple explanations for the trends in the calculated spin−orbital interaction energies in terms of chemical concepts (e.g., magnetic orbitals, overlap, and overlap density between magnetic orbitals, etc.) and geometrical parameters of spin exchange paths (e.g., M−O−M and M−O···O bond angles and O···O distance).[23,25] Though not impossible, it is very cumbersome to carry out similar analysis for a structurally complex magnetic solid such as $Fe_3O_2BO_3$ that has several unpaired spins per spin site and consists of several differently distorted spin sites. Thus, our discussion in the next section will focus on how the observed magnetic properties of $Fe_3O_2BO_3$ are related to the spin structure of its lattice predicted by the calculated spin−orbital interaction energies.

Table 4. Structural Features and Spin−Orbital Interaction Energies $\langle\Delta\epsilon\rangle$ of Various Spin Dimers in the 144 K Structure of $Fe_3O_2BO_3$

spin dimer	Fe···Fe (Å) (O···O)	interaction	oxygen sharing	$\langle\Delta\epsilon\rangle$ (meV)[a]
Interactions along the FeO_4 octahedral chains				
Fe(1)−Fe(1)	3.075	intrachain	edge	15.7
Fe(2)−Fe(2)	3.083	intrachain	edge	15.0 (12.1)
Fe(3)−Fe(3)	3.044	intrachain	edge	17.6
	3.106	intrachain	edge	14.2
Fe(4a)-Fe(4b)	3.077	intrachain	edge	3.1 (2.6)
Interactions within Each Fe/O Layer				
In the Fe(4a)−Fe(2)−Fe(4b) Sublattice				
Fe(2)−Fe(4a)	2.616	intratriad	edge	30.5 (30.5)
Fe(2)−Fe(4b)	2.942	intratriad	edge	2.3 (2.2)
Fe(4a)−Fe(4a)	6.141 (2.380)	intertriad	none	5.4 (7.1)
Fe(4b)-Fe(4b)	6.144 (2.373)	intertriad	none	5.0
In the Fe(3)−Fe(1)-Fe(3) Sublattice				
Fe(1)−Fe(3)	3.366	intratriad	corner	6.4
Fe(3)−Fe(3)	4.761 (2.384)	intertriad (//a)	none	1.2
Fe(3)−Fe(3)	5.552 (2.860)	intertriad (//b)	none	0.7
Between the Two Sublattices				
Fe(1)−Fe(4a)	3.116	intersublattice	edge	1.9 (2.0)
Fe(1)−Fe(4b)	3.085	intersublattice	edge	2.0
Fe(2)−Fe(3)	3.156	intersublattice	edge	2.8 (2.7)
	3.195	intersublattice	edge	2.5 (2.5)
Fe(3)−Fe(4a)	3.177	intersublattice	edge	2.5 (2.8)
Fe(3)−Fe(4b)	3.194	intersublattice	edge	1.4
Fe(3)−Fe(4a)	3.455	intersublattice	corner	7.5 (7.9)
Fe(3)−Fe(4b)	3.374	intersublattice	corner	5.4

[a] Each Fe(4a)−Fe(2)−Fe(4b) triad has one Fe^{2+} and two Fe^{3+} ions. The numbers without parentheses refer to the choice of Fe(2) as Fe^{2+}, and those in parentheses to that of Fe(4a) as Fe^{2+}.

In comparing the $\langle\Delta\epsilon\rangle$ values of superexchange (i.e., Fe−O−Fe) and super-superexchange (i.e., Fe−O···O−Fe) interactions in Tables 3 and 4, caution should be exercised. The J_F term is proportional to the exchange repulsion K_{12} between the two magnetic orbitals ϕ_1 and ϕ_2, that is, the Coulomb repulsion resulting from the overlap electron density distribution $\phi_1\phi_2$.[13,25] In the magnetic orbitals of a transition metal oxide, the d-orbitals of a metal ion are combined out-of-phase with the 2p-orbital of the surrounding oxygen atoms (i.e., "p-orbital tails"). The overlap density, and hence J_F, does not vanish when the p-orbital tails of the two magnetic orbitals are present on a common ligand atom as in corner- and edge-shared spin dimers (i.e., superexchange interactions) but practically vanishes when no ligand atom is shared between the two transition metal ions (i.e., super-superexchange interactions). Consequently, if

(32) Koo, H.-J.; Whangbo, M.-H. To be published.
(33) Smith, R. W.; Keszler, D. A. *J. Solid State Chem*. **1991**, *93*, 430.
(34) Miyahara, S.; Ueda, K. *Phys. Rev. B* **2000**, *61*, 3417.

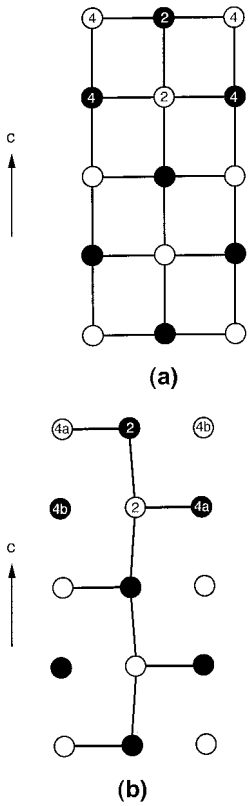

Figure 5. SISU in a chain made up of the Fe(4)−Fe(2)−Fe(4) triads in $Fe_3O_2BO_3$ at room temperature (a) and at 144 K (b). The filled and empty circles represent the iron sites with up and down spins, respectively, and each solid line between adjacent spin sites signifies the presence of strong antiferromagnetic spin exchange interaction. The SISU is an antiferromagnetic 3LL at room temperature and a symmetrically branched antiferromagnetic chain at 144 K.

superexchange and super-superexchange interactions had similar $\langle \Delta\epsilon \rangle$ values, the extent of antiferromagnetic interaction would be weaker in the superexchange path because the opposing effect of J_F is nonzero.[25]

5. Trends in Spin Exchange Interactions

In the present section, we probe the various questions raised in section 1 concerning the observed physical properties of $Fe_3O_2BO_3$. Our discussion is based on the spin−orbital interaction energies calculated for its crystal structures at room temperature and 144 K. These energies provide information about relative strengths of the nearest-neighbor spin exchange interactions of $Fe_3O_2BO_3$.

5.1. Above the Structural Phase Transition Temperature. Table 3 shows that above the structural phase transition temperature, the spin exchange interactions are substantially stronger along the FeO_4 chains than within each Fe/O layer. Only the intralayer/intratriad interactions of the Fe(4)−Fe(2)−Fe(4) sublattice are comparable in magnitude to the intrachain interactions. Consequently, as shown in Figure 5a, the strongly interacting spin units (SISUs) of the Fe(4)−Fe(2)−Fe(4) sublattice are 3LLs in which all nearest-neighbor spin sites are antiferromagnetically coupled. The intrachain interactions of the Fe(3)−Fe(1)−Fe(3) sublattice are comparable in strength to those of the Fe(4)−Fe(2)−Fe(4) sublattice. In the Fe(3)−Fe(1)−Fe(3) sublattice, however, the intralayer/intratriad interactions are much weaker than the intrachain interactions. Thus, the SISUs of this sublattice are given by linear antiferromagnetic chains along the *c*-direction.

5.2. Below the Structural Phase Transition Temperature. Table 4 shows that the structural phase transition substantially alters the spin exchange interactions in the Fe(4a)−Fe(2)−Fe(4b) sublattice. The intrachain Fe(2)−Fe(2) interaction is only slightly reduced by the structural transition. However, the Fe(4b)−Fe(2) intratriad as well as Fe(4a)−Fe(4b) intrachain interactions are strongly reduced, while the intratriad Fe(4a)−Fe(2) interaction becomes much stronger than the intrachain Fe(2)−Fe(2) interaction. Consequently, as shown in Figure 5b, the SISUs of the Fe(4a)−Fe(2)−Fe(4b) sublattice are symmetrically branched linear antiferromagnetic chains made up of the Fe(2)−Fe(4a) pairs. The SISUs of the Fe(3)−Fe(1)−Fe(3) sublattice are still given by linear antiferromagnetic chains.

In general, the spin exchange interactions between the Fe(4a)−Fe(2)−Fe(4b) and Fe(3)−Fe(1)−Fe(3) sublattices are considerably weaker than those within the SISUs of the two sublattices (see later for further discussion). This supports the suggestion that the two sublattices in $Fe_3O_2BO_3$ appear decoupled to a first approximation.[6]

Within each Fe/O layer, adjacent Fe(4a)−Fe(2)−Fe(4b) triads interact through the super-superexchange paths Fe(4a)−O···O−Fe(4a) and Fe(4b)−O···O−Fe(4b), where the O···O distance is 2.380 and 2.373 Å, respectively (see Table 4b and Figure 2b). Suppose that these intertriad interactions are antiferromagnetic. Then, as depicted in Figure 6a−c, adjacent SISUs (i.e., symmetrically branched linear antiferromagnetic chains made up of the Fe(2)−Fe(4a) pairs) become antiferromagnetically coupled to form a 3D antiferromagnetic lattice, while the Fe(4b) sites form isolated antiferromagnetc chains along the *b*-direction. Therefore, the antiferromagnetic transition of $Fe_3O_2BO_3$ at $T_N = 112$ K that takes place in the Fe(4a)−Fe(2)−Fe(4b) sublattice[6] should be related to the 3D antiferromagnetic ordering of the Fe(2)−Fe(4a) pairs. This antiferromagnetic transition is not seen by the macroscopic magnetic measurements but by the ^{57}Fe Mössbauer measurements.[6] This implies that there exists a weak component in the spin exchange interactions leading to the 3D antiferromagnetic ordering. This is indeed the case because the interactions between adjacent SISUs are considerably weak compared with those within each SISU.

The intra-SISU interactions of the Fe(3)−Fe(1)−Fe(3) sublattice are comparable in magnitude to the inter-SISU interactions of the Fe(4a)−Fe(2)−Fe(4b) sublattice, while the inter-SISU interactions of the Fe(3)−Fe(1)−Fe(3) sublattice are weak. Consequently, any long-range order (LRO) spin arrangement of the Fe(3)−Fe(1)−Fe(3) sublattice should be induced by the intersublattice interactions. Therefore, a fluctuation of spin arrangements would be likely in the Fe(3)−Fe(1)−Fe(3) sublattice above 70 K (i.e., the ordering temperature for the spins of the Fe(3)−Fe(1)−Fe(3) sublattice). In addition, a spin fluctuation is also likely at the Fe(4b) sites of the Fe(4a)−Fe(2)−Fe(4b) sublattice (see Figure 6a−

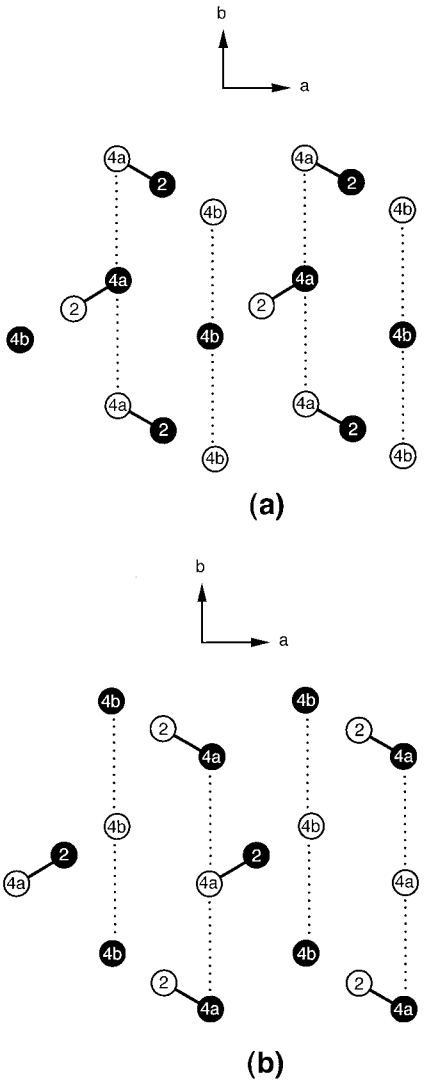

Figure 6. Antiferromagnetic spin arrangements of the SISUs in the Fe(4a)−Fe(2)−Fe(4b) lattice. Projection views of two successive Fe/O layers are given in (a, b). A perspective view of two adjacent SISUs is presented in (c). Each solid line between adjacent spin sites signifies the presence of strong antiferromagnetic spin exchange interaction, while the dotted lines represent the weak super-superexchange interaction Fe(4a)−O···O−Fe(4a) and Fe(4b)−O···O−Fe(4b).

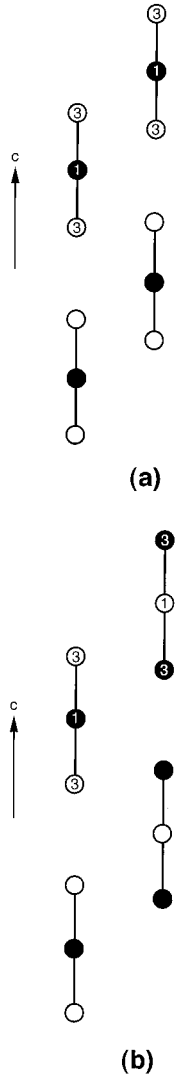

Figure 7. Projection views of the (a) ferromagnetic and (b) antiferromagnetic arrangements of the SISUs of the Fe(3)−Fe(1)−Fe(3) sublattice. Each circle represents the projection view of a linear antiferromagnetic chain along the *c*-direction, and within each Fe(3)−Fe(1)−Fe(3) triad, the adjacent SISUs are antiferromagnetically coupled.

c). This expectation is consistent with the finding that antiferromagnetism and paramagnetism coexist between 112 and 70 K.[6]

The EPR measurements of $Fe_3O_2BO_3$ show a single broad line in the temperature range 10−300 K.[10] The peak-to-peak line width ΔH_{pp} shows a plateau below 70 K but decreases gradually as the temperature is increased above 70 K. This unconventional temperature dependence of the line width is explained in terms of the spin fluctuation in the Fe(3)−Fe(1)−Fe(3) sublattice and in the Fe(4b) sites of the Fe(4a)−Fe(2)−Fe(4b) lattice, because the extent of the spin fluctuation should increase with increasing temperature. This is in support of Dumas et al.'s suggestion[10] that the single broad EPR line of $Fe_3O_2BO_3$ originates from the Fe^{2+} ions of the Fe(3)−Fe(1)−Fe(3) sublattice.

As already pointed out, the SISUs of the Fe(3)−Fe(1)−Fe(3) sublattice are linear antiferromagnetic chains (along the *c*-direction), which are coupled antiferromagnetically within each Fe(3)−Fe(1)−Fe(3) triad. The two LRO spin

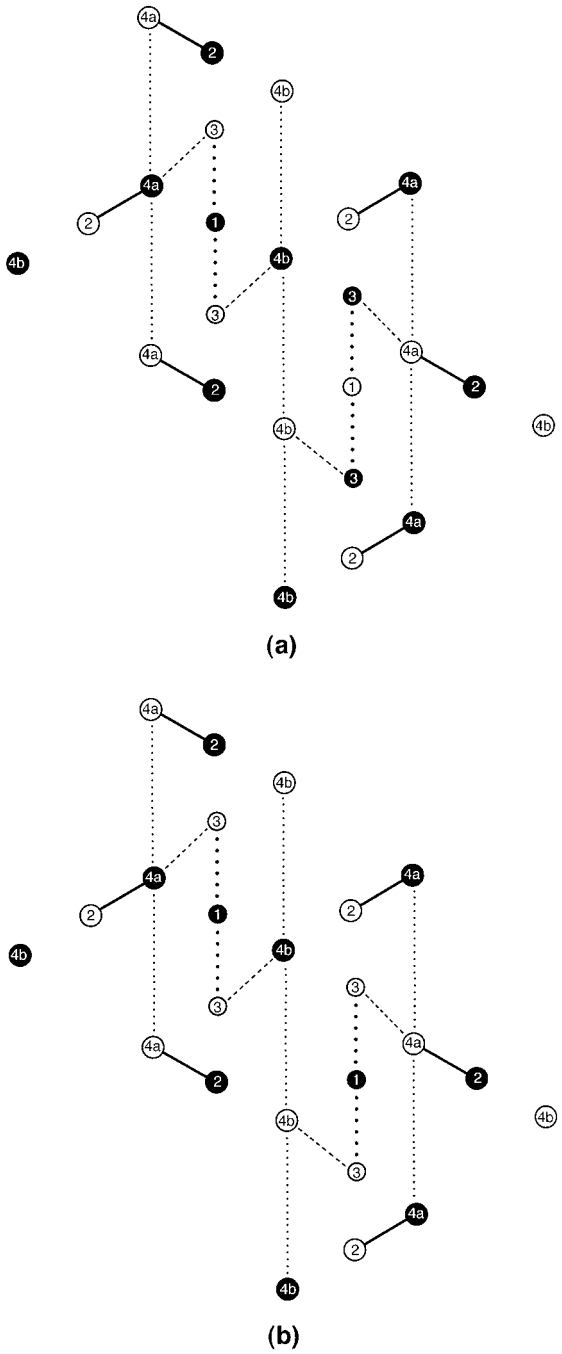

Figure 8. Interactions of two adjacent Fe(3)−Fe(1)−Fe(3) triads (connected by heavy dots) with the surrounding Fe(4a)−Fe(2)−Fe(4b) triads within an Fe/O layer. The dotted lines represent the super-superexchange interactions within the Fe(4a)−Fe(2)−Fe(4b) sublattice, and the dashed lines represent the interlattice interactions, that is, the Fe(3)−Fe(4a) and Fe(3)−Fe(4b) corner-sharing interactions. In (a), the two intersublattice interactions are antiferromagnetic for the two Fe(3)−Fe(1)−Fe(3) triads, thereby leading to an antiferromagnetic arrangement of the Fe(3)−Fe(1)−Fe(3) triads. In (b), the two intersublattice interactions are antiferromagnetic for one Fe(3)−Fe(1)−Fe(3) triad, but ferromagnetic for another, thereby leading to a ferromagnetic arrangement of the Fe(3)−Fe(1)−Fe(3) triads.

arrangements that these SISUs can adopt in this sublattice are the ferromagnetic arrangement (Figure 7a) and the antiferromagnetic arrangement (Figure 7b). Then, the weak ferromagnetism that sets in 70 K can be explained in terms of the ferromagnetic spin arrangement (Figure 7a) if the spins of the SISUs are canted to generate a small net magnetic moment. It is reasonable to suppose a spin canting in these SISUs because their high-spin Fe^{2+} ($S = 2$) ions have a nonspherical charge distribution and are, hence, subject to spin−orbit interaction and magnetic anisotropy.[35] The disappearance of the weak ferromagnetism below 40 K can be explained if the Fe(3)−Fe(1)−Fe(3) lattice adopts the antiferromagnetic spin arrangement (Figure 7b) so that no net magnetic moment results even when the spins of the SISUs are canted. It is of interest to consider how the spin arrangement of the Fe(3)−Fe(1)−Fe(3) sublattice can switch from ferromagnetic to antiferromagnetic. Table 4b shows that the intersublattice interactions take place through the Fe(3)−Fe(4a) and Fe(3)−Fe(4b) corner-sharing interactions. If these two interactions are antiferromagnetic throughout, the Fe(3)−Fe(1)−Fe(3) sublattice will have the antiferromagnetic spin arrangement, as indicated in Figure 8a. To have the ferromagnetic spin arrangement, the two intersublattice interactions should be antiferromagnetic in one column of Fe(3)−Fe(1)−Fe(3) triads and ferromagnetic in the neighboring column of Fe(3)−Fe(1)−Fe(3) triads, as indicated in Figure 8b.

6. Concluding Remarks

In understanding the puzzling magnetic properties of $Fe_3O_2BO_3$, it is crucial to find how the physical properties are related to its crystal structures. For the study of this structure−property correlation, it is necessary to estimate the relative strengths of various nearest-neighbor spin exchange interactions and examine how these interactions are affected by the structural phase transition. The method of spin dimer analysis presented in section 3 allows one to calculate spin−orbital interaction energies $\langle \Delta\epsilon \rangle$ for spin dimers that consist of octahedral spin sites containing different numbers of unpaired spins. These energies provide estimates for the relative strengths of the associated spin exchange interactions. The various physical properties of $Fe_3O_2BO_3$ are well accounted for in terms of the spin−orbital interaction energies calculated for its reported crystal structures above and below the structural phase transition temperature 283 K. Our present and previous studies[18−26] on various magnetic solids strongly suggest that the method of spin dimer analysis generalized in section 3 can be used to estimate the relative strengths of spin exchange interactions in complex magnetic solids and therefore predict the anisotropy of their magnetic properties. Our studies of many other magnetic solids, to be reported elsewhere,[32] show that this is indeed the case.

Acknowledgment. The work at North Carolina State University was supported by the Office of Basic Energy Sciences, Division of Materials Sciences, U.S. Department of Energy, under Grant DE-FG02-86ER45259.

IC010956Q

(35) Skomski, R.; Coey, J. M. D. *Permanent Magnetism*; Institute of Physics Publishing: Philadelphia, 1999; pp 12−14.